Microstructure changes in HPT-processed copper occurring at room temperature

P. Král[1*], J. Staněk[2], L. Kunčická[1], F. Seitl[2], L. Petrich[3], V. Schmidt[3], V. Beneš[2], V. Sklenička[1]

[1] Institute of Physics of Materials, ASCR, Zizkova 22, 616 62 Brno, Czech Republic

[2] Faculty of Mathematics and Physics, Charles University, Sokolovska 83, Prague, Czech Republic

[3] Institute of Stochastics, Ulm University, D-89069 Ulm, Germany

Abstract

In the present work the long-term stability of ultrafine-grained (UFG) copper at room temperature was investigated. The pure copper specimen was processed by 10 revolutions of high-pressure torsion (HPT) at room temperature. This procedure imposes an equivalent strain of about 300 to the material sample. In the region of these large strains a saturation in grain size refinement occurs. UFG copper, deformed up to the region of microstructure saturation, was subsequently annealed at room temperature for 6 years. Microstructure changes of HPT-processed copper were investigated by means of 2D and 3D electron back scatter diffraction (EBSD) and also by transmission electron microscopy.

It was found that the UFG microstructure of copper with saturated HPT-grain sizes coarsens significantly during long-term storage at room temperature. The analysis of grain volumes showed that the boundaries of coarse grains often contain flat segments with the coincidence site lattices (CSL) Σ3 and Σ9. The misorientation distributions revealed that most boundaries in the annealed microstructure are low energy grain boundaries of these kinds. However, groups of fine grains that are surrounded by random boundaries can also be found in the microstructure. Furthermore, 3D EBSD data were analysed in order to obtain a statistical microstructural information. The microstructure contains a high number of fine grains, but they form only a minority of the investigated volume. Quantitative geometrical characteristics of grain boundaries including CSL were described and interpreted.

Keywords: high-pressure torsion (HPT); ultrafine-grained microstructure; microstructure stability; 3D – electron back scatter diffraction; statistical image analysis.

*Corresponding author. Postal address: Zizkova 22, 61662 Brno, Czech Republic, Tel. +420-532 290 368, e-mail address: pkral@ipm.cz

1. Introduction

It is generally accepted that ultrafine-grained (UFG) or even nanocrystalline materials can be prepared in large volumes using methods of severe plastic deformation (SPD) [1-5]. Although various methods and their modifications have been developed, the most effective technique for production of UFG materials featuring very high imposed plastic strain is the high-pressure torsion (HPT) [6]. This method allows to introduce extremely large strains in a material even at cryogenic temperatures [7]. However, SPD-processed materials have a microstructure with low thermal stability and grains can coarsen even at room temperature (RT) [1,7].

It was found that microstructure stability of SPD processed materials depends on their purity, imposed equivalent strain and processing conditions such as temperature and applied pressure [7-14]. It was observed that the resistance against coarsening at RT decreases with decreasing melting temperature and stacking fault energy [15,16]. Thus the most susceptible materials to the microstructure coarsening at RT are materials such as Ag, Cu or Mg. Some works showed that the stability of SPD materials decreases with increasing values of imposed strain [7,13]. This result is reasonable because a high amount of stored energy (high density of lattice defects) in the microstructure after SPD generates a high driving force for recrystallization. However, in other works [10,11], it was observed that microstructure stability increases with increasing number of HPT turns and in the region of grain saturation (i.e. plastic strain more than 10-30) [17,18] it is more resistant against coarsening at room temperature than at low strains. But HPT discs of pure Cu after low strains exhibited significant softening predominantly near the edges

than in their central portions. The currently published works showed that SPD may have a different effect on microstructure stability at room temperature. The time-limited stability of microstructure and thus also properties of SPD-processed Cu at room temperature may influence any use of these materials in practice [14,19]. The detailed analysis of microstructure can contribute to a better understanding to the microstructure stability at room temperature. Thus, the aim of the present work is the characterization of microstructure changes in pure copper deformed up to the region of grain size saturation after long-term annealing at RT using 2D and 3D – electron back scatter diffraction (EBSD). The quantitative description of the microstructure extends the results presented in [20].

2. Experimental material and procedures

The experimental material used in present work was ultrafine-grained Cu. The 20 mm diameter discs with 1 mm thickness were manufactured from an ingot of cast Cu with a purity slightly better than 99.99wt.% (chemical composition in Table 1) and a mean grain size of about 1.2 mm. The specimens were subjected to 10 HPT revolutions at room temperature under a pressure of 4 GPa. The equivalent von Mises strain (ε_{eq}) imposed by the HPT processing can be calculated according to the following equation [1]:

$$\varepsilon_{eq} = \gamma/\sqrt{3} = 2\pi rN/\sqrt{3}t \quad (1)$$

where γ is shear strain, r is the distance from the torsion axis, N is the number of turns, and t is the thickness of the disc.

The Cu samples were subsequently annealed at room temperature for about 6 years. Their microstructure was examined in 2D and 3D by a FIB/SEM Tescan Lyra 3 equipped with an EBSD detector manufactured by Oxford Instruments. The 3D scans were performed fully automatically using a focused ion beam (FIB) for milling and EBSD for microstructure analysis without the necessity of specimen repositioning, see [21,22]. The EBSD analyses were

performed in the sections of the torsion axis. The microstructure in 2D and 3D was investigated in areas of about $20\times15\ \mu m^2$ with a step size for the EBSD mapping of 80 nm. The reconstruction of the 3D structures from the individual 2D slices and the determination of grains and their characteristics was performed using the software DREAM-3D, see [23]. Grains were characterized as the volumes (areas in 2D) completely surrounded by boundaries with misorienation angles $\theta > 15°$.

Additional microstructure investigations were performed by transmission electron microscopy (TEM). The TEM studies were carried out on thin foils using a JEOL 2100 F microscope operating at 200 kV.

3. Results

3.1. Microstructure of pure Cu after HPT

Fig. 1a shows the microstructure of a Cu sample processed by 10 HPT revolutions. One can see that the microstructure is more or less homogeneous. The grain size distribution revealed that most grains had a size of about 0.4 μm (Fig. 1b) but there were also grains whose sizes exceeded the 1 μm mark.

The misorientation distribution shows that the microstructure contains predominantly high-angle grain boundaries (HAGB) (Fig. 1c). Approximately 78% of grain boundaries in the microstructure are HAGBs. These are distributed similar to the Mackenzie plot of the misorientation distribution for a sample with a random texture. However, in the interior of a few larger grains, there were observed low-angle grain boundaries with misorientation lower than 15° (Fig. 1c).

Fig. 1d shows the distribution of the strains in the HPT-processed Cu using local changes of misorientation. It can be seen that the distribution of local misorientation is heterogeneous not only in the microstructure, but also in the interior of the individual grains. The results

demonstrate that predominantly grains with high values of local misorientation can be observed in the microstructure. The highest values of local misorientation were often detected near boundaries and triple points. However, grains with local misorientation values, which are small compared to the local misorientation values of neighbouring grains, can be found in the microstructure, too.

3.2. Microstructure of pure Cu after HPT and long-term annealing

Fig. 2a shows the microstructure of HPT-processed Cu after long-term annealing at room temperature. The results demonstrate the significant coarsening of grains, resulting in the duplex microstructure containing large and fine grains in comparison with the microstructure before annealing. The large grains reached sizes of about 3 μm (Fig. 2b).

The misorientation distribution (Fig. 2c) demonstrates that the microstructure after long-term annealing contains predominantly HAGBs. The majority of HAGBs are formed by special boundaries Σ3 (111/60°) and Σ9 (110/38.94°). These boundaries form the prevalent part of large grain boundaries. However, fine grains are predominantly surrounded by random boundaries. The distribution of local orientation changes in the microstructure (Fig. 2d) revealed a significant decrease of areas with high values of local misorientation in comparison to the microstructure before annealing. The majority of areas (more than 90%) exhibits the local misorientation up to 0.5°.

Fig. 3 shows that large grains exceeding 1 μm are predominantly surrounded by straight segments of different lengths. The results demonstrate that the boundaries of large grains can have step-like character. Groups of small grains with rounded boundaries can also be seen in the microstructure (Fig. 3b).

3.3. 3D EBSD results

In order to obtain more information on microstructure changes and the distribution of boundaries, the microstructure was investigated in 3D. We use a specimen of the size 8x8x2.88 μm - (Fig. 4). Fig. 5 demonstrates selected individual slices of the 3D EBSD map from Fig. 4a.

Detailed investigation of microstructure changes in 2D slices of the 3D EBSD map revealed that separated fine grains (denoted A,B) are situated in the interior of a large (blue) grain, marked by 1, see Fig. 5 a,b. It is seen that the fine grain A in Fig. 5 a is surrounded by Σ3 boundary, but the fine grain B visualized in Fig. 5 b has a random boundary. Further 2D slices (Fig. 5 c,d) showed that the grains are not situated in the interior of the large grain volume, but they are also connected with other grains. The results demonstrate that the boundaries of these grains change their misorientation in transition from one neighbouring grain to another one (e.g. grain A in Fig. 5 a,b). The Σ3 boundaries enclosing the grain A are partially transformed into the boundary Σ9 (Fig. 5 b). The random boundary of grain B is partially transformed into the special boundary Σ3 (Fig. 5 c,d). Similar misorientation changes (denoted by white arrows) in parts of the grain boundaries can be observed in other selected slices, too (Fig. 5 a-d).

The 2D slices show that the large blue grain 1 in Fig. 5 a,b is replaced by several finer grains, see Fig. 5 c,d. However, the 3D EBSD map reconstructed from 2D slices revealed that the large blue grain 1 has a very rugged surface, so that in some 2D slices it can be seen as several finer grains (Fig. 5,6).

3.4. Quantitative characteristics of the microstructure

The 3D EBSD map was analysed separately, using the software DREAM3D, see [23]. Besides the local phenomena described in the previous sections, this approach allows us to obtain global statistical information about the specimen. For this purpose, we work with a larger specimen than in the preview section, more precisely with a specimen of the size 18.88x14x5.88 μm. For

detection of individual grains, we use the filter 'Segment Features (Misorientation)' in DREAM.3D with misorientation tolerance of 2 degree, see Fig. 7. In this section we present some quantitative geometrical characteristics of the specimen with an emphasis on grain boundaries.

There are 2265 grains in the sample (edge effects are not corrected), the majority of them is very fine, so that the 95 biggest grains form 75% of the overall volume. In Fig. 8, histograms of various grain characteristics are shown: volume (Vol), sphericity (Sph) and number of neighbouring grains (Nng). The number of neighbouring grains is equal to the number of faces of the grain under consideration. Note that the faces of a grain form the grain boundary. The empirical correlation coefficients between Vol-Sph, Vol-Nng and Sph-Nng are -0.29 (i.e., the bigger grains are less likely spherical), 0.76 (i.e., the bigger the grain is the more neighbours it has), -0.44 (i.e., the more spherical grains have smaller numbers of neighbours), respectively.

Further analysis concerns the grain faces and their misorientations. There is 11513 faces in the sample, among them 1458 faces with the largest surface areas form 75% of the total surface area.

For a face we define its volume neighbour ratio (VNR) by the formula

$$VNR = \left(\frac{max(|C_1|,|C_2|)}{min(|C_1|,|C_2|)} - 1\right)^{1/2}, \qquad (2)$$

where C_1, C_2 are the neighbouring grains of the considered (common) face and $|C|$ denotes the volume of set C. Note that the VNR encounters interactions between the volumes of neighbouring grains, where it is equal to zero when the volumes are equal, otherwise it is positive. In Fig. 9 we present histograms of misorientation, surface area and VNR for all faces and the largest ones, respectively. As seen from the figure, many of the faces with largest surface are Σ3 boundaries (approximately 30%). On the other hand, misorientation of all faces together is distributed more uniformly. In this case, only 10% of the boundaries are Σ3. As in Fig. 2c, the misorientation histograms reveal peaks corresponding to Σ3 and Σ9 boundaries. Our

aim is to classify their spatial distribution. For this purpose, we assign a location to each face, i.e. we consider the point

$$\left[x_1 + \frac{ed_1}{ed_1+ed_2}(x_2 - x_1), y_1 + \frac{ed_1}{ed_1+ed_2}(y_2 - y_1), z_1 + \frac{ed_1}{ed_1+ed_2}(z_2 - z_1)\right], \quad (3)$$

where $[x_i, y_i, z_i]$ are the coordinates of the centroid of the face and ed_i denotes the volume-equivalent diameter, i = 1,2, of the neighbouring grains. In this way, a point pattern is formed in 3D.

The faces with misorientations lower than 15 degrees are omitted. Those with higher misorientation are splitted into 3 groups: Σ3 (I) and Σ9 (II) boundaries, and the rest creates the third group (III). Σ3 boundaries are considered as those with misorientations of 60±2 degrees, and Σ9 boundaries those with misorientations of 39±2 degrees. Thus, we obtain three point patterns: (I), (II), (III), where the number of points is equal to 1508, 1289, 7795, respectively. Plots of these three point patterns are shown in Fig. 10.

We now investigate the spatial distributions of the special boundaries Σ3 and Σ9. In Fig. 11, three characteristics of the point patterns (I), (II), and (III) are considered, namely the empty-space function (called F-function for brevity), the nearest-neighbour distance distribution function (briefly called G-Function), and the pair correlation function (briefly called g-function), cf. [24]. The empty-space function is the cumulative distribution function (cdf) of the radius of a randomly located sphere, when it first hit a point of the considered point pattern. Similarly, the nearest-neighbour distance distribution function is the cdf of the distance between a randomly selected point of the considered point pattern and its nearest neighbor in the pattern. The pair correlation function describes the (normalized) frequencies of distances between pairs of points, where values higher/smaller than one indicate that the considered distance is more/less likely than in the model of complete spatial randomness. These three characteristics are estimated for each point pattern (I), (II), (III) and plotted together with the corresponding

(theoretical) characteristics for the Poisson point process, which represents complete spatial randomness (CSR). The graphs reveal some clustering in all three point patterns, in particular, this means that special boundaries are clustered. The points are not scattered completely at random in the 3D space which is caused by the presence of large grains (there are no points in their interior). Comparing the integrated distance between both (solid and dashed) curves in the plots for the F-function and the G-function in Fig. 11, we observe that the clustering is slightly weaker for point pattern (I) than for point pattern (II), which, in addition, is confirmed by comparing the maximum values of the g-functions for (I) and (II).

This is confirmed by Fig. 12, histograms I-II and II-I, where the distances taken from a point of one pattern to the nearest neighbour of the other pattern are considered.

Note that the present statistical 3D analysis of grain boundaries is more comprehensive than that one performed in [21].

4. Discussion

The grain refinement of pure metals after substantially large imposed strains usually reaches the state of saturation and further increase in strain does not significantly contribute to additional reduction of the grain size [17,18]. The processing of copper of 99.99% purity by 10 HPT revolutions at room led to the introduction of plastic strain of about 300 into the material which led to the transformation of the initial coarse-grained Cu microstructure to an ultrafine-grained one. The mean grain size of HPT-processed Cu was about 0.42 μm. Fig. 13 shows the comparison of mean grain size measured in the present work with the results published in previous studies [10,12,25-29]. The value of mean grain size in the present work is comparable to the previously published results for the grain size determined by the EBSD method [10,25]. The results also demonstrate that the values of mean grain size measured by TEM or SEM (back scattered electron micrographs) are smaller in comparison with EBSD

results. The reason for this difference is that TEM and SEM measure often all detectable boundaries, while EBSD measures only the boundaries defined by characteristic misorientation for HAGBs. For this reason, some works designated the microstructure region measured by TEM or SEM as crystallite [27] or element size [12].

Previous studies [7,10,14] revealed that the microstructure of pure SPD-processed Cu is unstable even at room temperature. It has been found that the largest changes of hardness and microstructure occur up to equivalent strain about 10. These phenomena can be attributed to the formation of UFG structure during SPD processing. At very low equivalent strains, the substructure starts to develop, the dislocation density increases, dislocation tangles and dislocation walls are created, and the microstructures are predominantly formed by LAGBs surrounding the newly occurring subgrains [30,31,32]. The value of LAGBs and dislocation density decreases with further increase of equivalent strain. Subgrains are subsequently transformed into grains and dislocations moved from their interiors to boundaries. Strains higher than about 10 lead to an equilibrium between the generation and annihilation of defects and the microstructure characteristics (such as grain size and number of HAGBs) saturate at a certain value [17,18]. It was observed that the microstructure of Cu processed by HPT up to region of refinement saturation exhibited only minor changes of microstructure and hardness even after long-term annealing at RT [7,10].

The formation of UFG microstructure occurs under high external stresses, which cause plastic strain. The high stress and strain applied in the region of saturation leads to the strain-induced boundary migration [17,33]. The results obtained in the present work show that internal microstrain, indicated by changes in local misorientation, is distributed heterogeneously in the microstructure. The largest values of local misorientation were found near grain boundaries, which can be caused by pileups of dislocations and by unrecovered dislocation entering into the boundaries. In the microstructure, also grains with low values of local misorientation were

observed. The regions with different values of local misorientation may serve as nucleation places for grain coarsening during long-term annealing at room temperature. It is generally accepted that the heterogeneity of strain plays an important role in grain coarsening. It was found that in the specimens processed by equal-channel angular pressing (ECAP), the grains predominantly coarsen only in certain areas of the ECAP specimen [13,14,34]. However, the plastic strain is not fully homogeneous, also in specimens processed by HPT, because the strain depends on the radius according to Eq. (1). For this reason, the same microheterogeneity of strain may be expected in HPT processed specimens.

The results obtained in the present work demonstrate that long-term annealing at room temperature of HPT-processed Cu led to the formation of large grains with low values of local misorientation i.e. with low density of geometrically necessary dislocations. The increase of area with low local misorientation is caused by the boundary migration from low into the high dislocation region. Thus, the deformed microstructure formed during the HPT process is replaced by a recrystallized one.

The comparison of misorientation distributions before and after annealing revealed that random boundaries are replaced by low energy boundaries, predominantly by Σ3 and Σ9. Furthermore, the results demonstrate that the replacement of random boundaries by special ones led to a reduction in the overall boundary curvature because special boundaries are formed by straight segments. The special boundaries Σ3 and Σ9 are very often combined with each other. The boundary Σ9 is often split into two Σ3 boundaries, but in the whole space of the specimen, the locations of Σ9 boundaries are slightly more clustered than the locations of Σ3 boundaries. It can be suggested that the transformation of curved grain boundaries into flat areas is a consequence of reducing the energy of deformed microstructure [35,36], when the original boundaries may even be in a non-equilibrium state [1].

The 3D EBSD results show that the annealed microstructure contains quite large grains with significantly irregular shapes. The irregular surface of coarse grains in the annealed microstructure is probably influenced by the heterogeneous distribution of local misorientation created during HPT. For this reason the grains grow in various deformed volumes at different rates.

It was found that less than 5% of all grains occupy about 75% of the whole volume. The rest of volume is formed by very fine grains, which were probably inherited from the initial HPT microstructure. The 3D plot of point patterns shown in Fig. 10 demonstrates that grain faces are distributed inhomogeneously in the volume, which implies an inhomogeneous distribution of fine grains. This can influence the local strength of the annealed specimen. Fig. 14 shows results of the measurements of hardness from the centre to the edge of the annealed disc. It can be seen that the hardness of annealed UFG Cu exhibited a significant scattering of the measured values. Previous works [10,11,15,16] showed that the hardness of 99.99% Cu deformed up to the region of microstructure saturation is unchanged after short-term annealing at RT but slight decrease of hardness was observed after long-term annealing (Fig. 14). It was found [37] that RT stability of UFG Cu is significantly reduced by additional rolling deformation because the various deformation modes led to the formation of new microstructure heterogeneities. It can be suggested that microstructure heterogeneities in HPT-processed Cu, investigated in the present work, probably caused lower RT stability in comparison with the results published in other works [7,10]. The RT stability of microstructure and hardness of HPT-processed Cu investigated in the present work may also be influenced by the slightly different content of impurities in comparison with chemical composition published in ref. [10,38]. Zhang et al. [39] reveled that microstructure stability of HPT-processed material can be influenced not only by its purity but also significantly by the kind of solute atoms.

5. Conclusion

The microstructure of UFG pure Cu processed by HPT up to the region of grain size saturation is not stable and grains can coarsen even at room temperature. The large grains are surrounded by segments of special boundaries. 3D EBSD analyses revealed that the annealed microstructure can contain a high number of fine grains, but the coarse grains occupy the majority of the investigated volume. The statistical analysis of the 3D microstructure performed in this work provided additional information about the microstructure and, in this way, clarified some experimental observations of the microstructure changes.

Acknowledgement

The authors acknowledge the financial support for this work provided by the Czech Science Foundation, project 17-00393J.

References

[1] R.Z. Valiev, R.K. Islamgaliev, I.V. Alexandrov, Bulk nanostructured materials from severe plastic materials, Prog. Mater. Sci. 45 (2000) 103-189. https://doi.org/10.1016/S0079-6425(99)00007-9.

[2] T. Fujioka, Z. Horita, Development of high-pressure sliding process for microstructural refinement of rectangular metallic sheets, Mater. Trans. 50 (2009) 930-933. http://doi.org/10.2320/matertrans.MRP2008445.

[3] G. Faraji, M. M. Mashhadi, H. S. Kim, Tubular channel angular pressing (TCAP) as a novel severe plastic deformation method for cylindrical tubes, Materials Letters 65 (2011) 3009-3012. http://dx.doi.org/10.1016/j.matlet.2011.06.039.

[4] R. Kocich, L. Kunčická, A. Macháčková, Twist Channel Multi-Angular Pressing (TCMAP) as a method for increasing the efficiency of SPD, IOP Conf. Ser. Mater. Sci. Eng. 63 (2014) 12006. http://doi.org/10.1088/1757-899X/63/1/012006

[5] L. Kunčická, R. Kocich, P. Král, M. Pohludka, M. Marek, Effect of strain path on severely deformed aluminium, Materials Letters 180 (2016) 280–283. http://dx.doi.org/10.1016/j.matlet.2016.05.163.

[6] L. Kunčická, T.C. Lowe, C.F. Davis, R. Kocich, M. Pohludka, Synthesis of an Al/Al2O3 composite by severe plastic deformation, Mater. Sci. Eng. A. 646 (2015) 234–241. doi:10.1016/j.msea.2015.08.075

[7] K. Edalati, J. M. Cubero-Sesin, A. Alhamidi, I. F. Mohamed, Z. Horita, Influence of severe plastic deformation at cryogenic temperature on grain refinement and softening of pure metals: Investigation using high-pressure torsion, Mater. Sci. Eng. A 613 (2014) 103–110. http://dx.doi.org/10.1016/j.msea.2014.06.084.

[8] J. Gubicza, N. Q. Chinh, J. L. Lábár, Z. Hegedüs, T.G. Langdon, Principles of self-annealing in silver processed by equal-channel angular pressing: The signifikance of a very low stacking fault energy. Mater. Sci. Eng. A 527 (2010) 752-760. http://dx.doi.org/10.1016/j.msea.2009.08.071.

[9] T. Konkova, S. Mironov, A. Korynikov, S.L. Semiatin, On the room-temperature annealing of cryogenically rolled copper, Mater. Sci. Eng. A 528 (2011) 7432-7443. http://dx.doi.org/10.1016/j.msea.2011.06.047.

[10] Y. Huang, S. Sabbaghianrad, A.I. Almazrouee, K.J. Al-Fadhalah, S.N. Alhajeri, T.G. Langdon, The significance of self-annealing at room temperature in high-purity copper processed by high-pressure torsion, Mater. Sci. Eng. A 656 (2016) 55-66. http://dx.doi.org/10.1016/j.msea.2016.01.027.

[11] A.I. Almazrouee, K.J. Al-Fadhalah, S.N. Alhajeri, Y. Huang, T.G. Langdon, Effect of long-term storage on microstructure and microhardness stability in OFHC Copper processed by high-pressure torsion, Adv. Eng. Mater. (2019) http://dx.doi.org/10.1002/adem.201801300.

[12] T. Hebesberger, H.P. Stüwe, A. Vorhauer, F. Wetscher, R. Pippan, Structure of Cu deformed by high pressure torsion, Acta Mater. 53 (2005) 393–402. http://dx.doi.org/10.1016/j.actamat.2004.09.043

[13] M. Kawasaki, Z. Horita, T.G. Langdon, Microstructural evolution in high purity aluminium processed by ECAP, Mater. Sci. Eng. A 524 (2009) 143-150. http://dx.doi.org/10.1016/j.msea.2009.06.032.

[14] P. Král, J. Dvořák, M. Kvapilová, W. Blum, V. Sklenička, The influence of long-term annealing at room temperature on creep behaviour of ECAP-processed copper, Mater. Letters 188 (2017) 235–238. http://dx.doi.org/10.1016/j.matlet.2016.11.002.

[15] H. Matsunaga, Z. Horita, Softening and microstructural coarsening without twin formation in FCC metals with Low Stacking Fault Energy after Processing by High-Pressure Torsion, Mater. Trans. 50 (2009) 1633-1637. http://dx.doi.org/ 10.2320/matertrans.MF200921.

[16] K. Edalati, Y. Hashiguchi, H. Iwaoka, H. Matsunaga, R.Z. Valiev, Z. Horita, Long-time stability of metals after severe plastic deformation: Softening and hardening by self-annealing versus thermal stability, Mater. Sci. Eng. A 729 (2018) 340–348. https://doi.org/10.1016/j.msea.2018.05.079.

[17] R. Pippan, S. Scheriau, A. Taylor, M. Hafok, A. Hohenwarter, A. Bachmaier, Saturation of fragmentation during severe plastic deformation, Annu. Rev. Mater. Res. 40 (2010) 319–343. http://dx.doi.org/10.1146/annurev-matsci-070909-104445.

[18] B. B. Straumal, A. R. Kilmametov, Y. Ivanisenko, A. A. Mazilkin, O. A. Kogtenkova, L. Kurmanaeva, A. Korneva, P. Zieba, B. Baretzky, Phase transitions induced by severe plastic deformation: steady-state and equifinality, Int. J. Mater. Res. (formerly Z. Metallkd.) 106 (2015) 657-664. http://dx.doi.org/10.3139/146.111215.

[19] P.-L. Pai, C. H. Ting, Copper as the future interconnection material. Proceedings of the Sixth International IEEE VLSI Multilevel Interconnection Conference (1989) 258-264.

[20] O. Šedivý, V. Beneš. P. Ponížil, P. Král, V. Sklenička, Quantitative characterization of microstructure of pure copper processed by ECAP. Image Anal. Stereol. 32 (2013) 65-75. http://dx.doi.org/10.5566/ias.v32.

[21] A. J. Schwartz, M. Kumar, B. L. Adams, D. P. Field (eds.) 2009 Three –Dimensional orientation microscopy by serial sectioning and EBSD-based orientation mapping in a FIB-SEM (Electron Backscatter Diffraction in Material Science) New York: Springer Science+Business Media, chapter 8, 109-122.

[22] P. Král, J. Dluhoš, P. Peřina, T. Barták, 3D analysis of microstructure changes occurring during creep tests of ultra-fine grained materials. Mater. Sci. Forum 753 (2013) 46-49. http://dx.doi.org/10.4028/www.scientific.net/MSF.753.46.

[23] M.A. Groeber, M.A. Jackson, DREAM.3D: A digital representation environment for the analysis of microstructure in 3D. Integrating Materials (2014) 3: 5. https://doi.org/10.1186/2193-9772-3-5.

[24] S.N. Chiu, D. Stoyan, W.S. Kendall, J. Mecke 2013 Stochastic Geometry and its Applications. 3rd Ed., Wiley, Chichester.

[25] X. Molodova, G. Gottstein, M. Winning, R.J. Hellmig, Thermal stability of ECAP processed pure copper, Mater. Sci. Eng. A 460–461 (2007) 204–213. http://dx.doi.org/10.1016/j.msea.2007.01.042.

[26] P. Lukáš, L. Kunz, M. Svoboda, Fatigue mechanisms in ultrafine-grained copper, Kovove Mater. 47 (2009) 1–9.

[27] W. Blum, Y.J. Li, Y. Zhang, J.T. Wang, Deformation resistance in the transition from coarse-grained to ultrafine-grained Cu by severe plastic deformation up to 24 passes of ECAP, Mater. Sci. Eng. A 528 (2011) 8621– 8627. https://doi.org/10.1016/j.msea.2011.08.010.

[28] K. Edalati, T. Fujioka, Z. Horita, Microstructure and mechanical properties of pure Cu processed by high-pressure torsion Mater. Sci. Eng. A 497 (2008) 168–173. http://dx.doi.org/10.1016/j.msea.2008.06.039.

[29] Z.L. Xie, J.J. Xie, Y.S. Hong, X.L. Wu, Influence of processing temperature on microstructure and microhardness of copper subjected to high-pressure torsion, Sci. China Tech. Sci. 53 (2010) 1534−1539. http://dx.doi.org/10.1007/s11431-010-3157-7.

[30] F.J. Humphreys, M. Hetherly, Recrystallization and Related Annealing Phenomena, 2nd ed., Elsevier Ltd, Oxford, 2004.

[31] B. Verlinden, J. Driver, I. Samajdar, R.D. Doherty, Thermo-mechanical processing of metallic materials, Elsevier, Amsterdam, 2007.

[32] R. Kocich, M. Kursa, I. Szurman, A. Dlouhý, The influence of imposed strain on the development of microstructure and transformation characteristics of Ni–Ti shape memory alloys, J. Alloys Compd. 509 (2011) 2716–2722. doi:10.1016/j.jallcom.2010.12.003

[33] A. Vorhauer, R. Pippan, On the onset of a steady state in body-centered cubic iron during severe plastic deformation at low homologous temperatures, Metall. Mater. Trans. A 39 (2008) 417-429. http://dx.doi.org/10.1007/s11661-007-9413-1.

[34] P. Král, W. Blum, J. Dvořák, P. Eisenlohr, M. Petrenec, V. Sklenička, Dynamic restoration of severely predeformed, ultrafine-grained pure Cu at 373K observed in situ, Mater. Character. 134 (2017) 329-334. https://doi.org/10.1016/j.matchar.2017.11.006.

[35] B. B. Straumal, S. A. Polyakov, E. Bischoff, W. Gust, E. J. Mittemeijer, Faceting of Σ3 and Σ9 grain boundaries in copper, Interface Science 9 (2001) 287–292. https://doi.org/10.1023/A:1015174921561.

[36] B.B. Straumal, S.A. Polyakov, E.J. Mittemeijer, Temperature influence on the faceting of Σ3 and Σ9 grain boundaries in Cu, Acta Mater. 54 (2006) 167–172. http://dx.doi.org/10.1016/j.actamat.2005.08.037.

[37] O.V. Mishin, G. Gottstein, Microstructural aspects of rolling deformation in ultrafine-grained copper, Phil. Mag. A 78 (1998) 373-388. http://dx.doi.org/ 10.1080/01418619808241909.

[38] A.I. Almazrouee, K.J. Al-Fadhalah, S.N. Alhajeri, T.G. Langdon, Microstructure and microhardness of OFHC copper processed by high-pressure torsion, Mater. Sci. Eng. A 641 (2015) 21–28. http://dx.doi.org/10.1016/j.msea.2015.06.016.

[39] H.W. Zhang, K. Lu, R. Pippan, X. Huang, N. Hansen, Enhancement of strength and stability of nanostructured Ni by small amounts of solutes, Scripta Mater. 65 (2011) 481–484. http://dx.doi.org/10.1016/j.scriptamat.2011.06.003.

Figure captions

Fig. 1 Microstructure of pure Cu processed by 10 HPT revolutions: a) inverse pole figure map, b) distribution of grain sizes, c) misorientation distribution of boundaries, d) local misorientation map (the colour scale is in degrees).

Fig. 2 Microstructure of HPT-processed Cu after long-term annealing at RT: a) inverse pole figure map (special boundaries Σ3 (white) and Σ9 (brown) and random boundaries (black)), b) distribution of grain sizes, c) misorientation distribution of boundaries, d) local misorientation map (the colour scale is in degrees).

Fig. 3 TEM micrographs of annealed Cu a) segmented boundary of large grains, b) duplex microstructure of large faceted grains and fine grains.

Fig. 4 3D EBSD reconstruction of an RT annealed microstructure

Fig. 5 Selected 2D slices from a 3D EBSD map (Fig. 4). Coloured boundaries indicate special boundaries (Σ3 white, Σ9 brown), black boundaries indicate random boundaries.

Fig. 6 Grain 1 from the 3D EBSD map reconstructed from 2D slices

Fig. 7 3D microstructure of pure Cu after HPT and long-term annealing (grains coloured at random).

Fig. 8 Histograms of 3D grain characteristics of the sample shown in Fig. 7: volume [μm^3], sphericity, number of neighbours.

Fig. 9 Histograms of 3D characteristics of grain boundaries (faces) of the sample shown in Fig. 7: misorientation [degrees], surface area [μm^2], VNR defined in (2). The histograms are computed a) from all 11513 faces, and b) from the 1458 faces with the biggest surface areas. The largest surface is 67.83 μm^2, but only 40 faces have surface area larger than 10 μm^2. Therefore histograms of face area do not display 0.35 % of faces in the case a) and 2.74 % of faces in the case b).

Fig. 10 3D plots of the point patterns (I) – red, (II) – green and (III)-black, corresponding to the locations of grain faces.

Fig. 11 Spatial distribution of grain boundaries: F-function, G-function and g-function of the point patterns (I), (II), and (III) (estimated with correction of edge effects, solid lines) and of the completely random model (dashed lines).

Fig. 12 Histograms of cross-nearest-neighbour distances, for pairs of points from (I), (II), and (III). The heavier tail in histogram I-II in comparison to histogram II-I indicates that pattern (II) is slightly more clustered than (I). Note that the histograms regarding pattern (III) are influenced by a larger difference between the number of points of the respective pairs of point patterns.

Fig. 13 Comparison of mean grain size measured in the present work with results published in previous works

Fig. 14 Comparison of microhardness measured in the present work with results published in previous works

Table captions

Table 1. Chemical composition of investigated Cu (in wt%). The balance is copper.

Material	Sb	As	Fe	Ni	Pb	Sn	P	Ag	Zn
Cu99.99	0,0002	<0,0004	0,0005	<0,0001	<0,0001	<0,0003	<0,001	0,0018	<0,0002

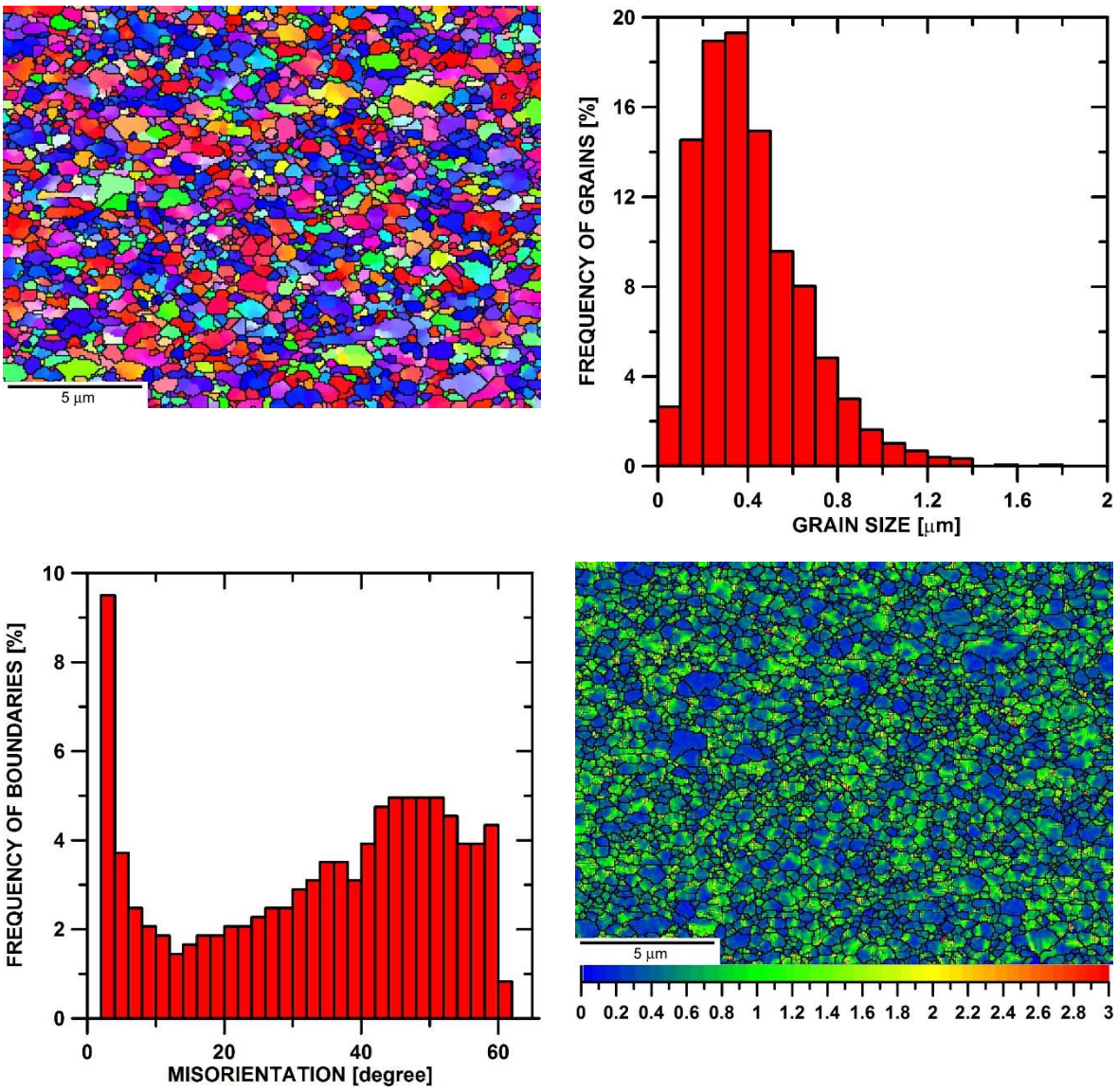

Fig. 1 Microstructure of pure Cu processed by 10 HPT revolutions: a) inverse pole figure map, b) distribution of grain sizes, c) misorientation distribution of boundaries, d) local misorientation map (the colour scale is in degrees).

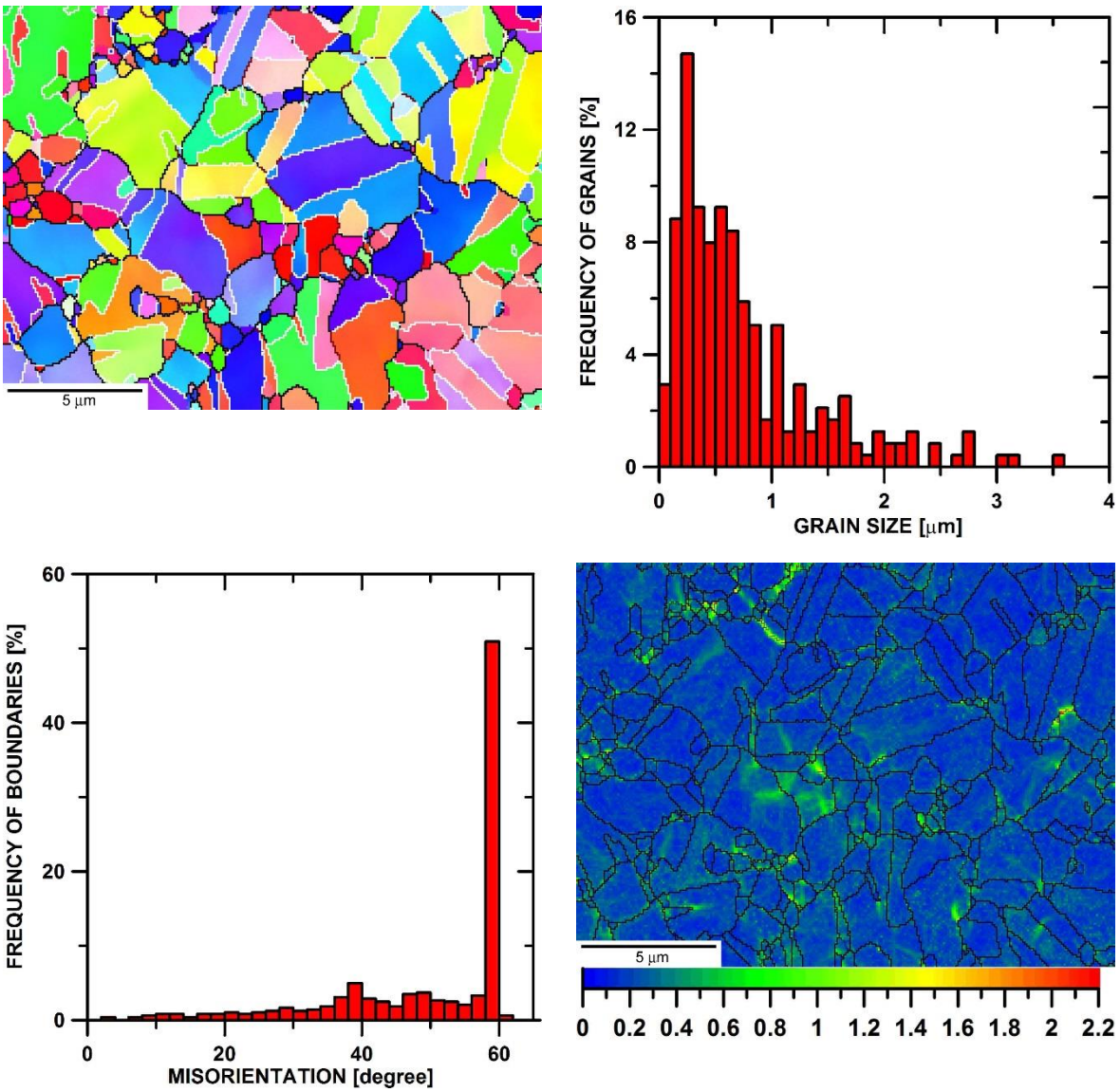

Fig. 2 Microstructure of HPT-processed Cu after long-term annealing at RT: a) inverse pole figure map (special boundaries Σ3 (white) and Σ9 (brown) and random boundaries (black)), b) distribution of grain sizes, c) misorientation distribution of boundaries, d) local misorientation map (the colour scale is in degrees).

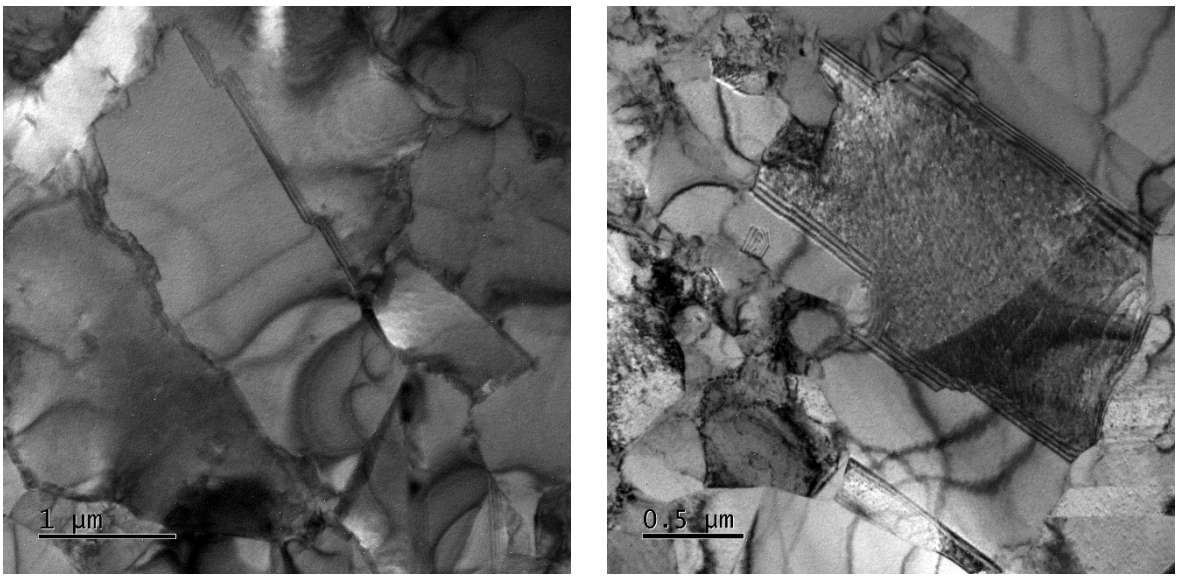

Fig. 3 TEM micrographs of annealed Cu a) segmented boundary of large grains, b) duplex microstructure of large faceted grains and fine grains.

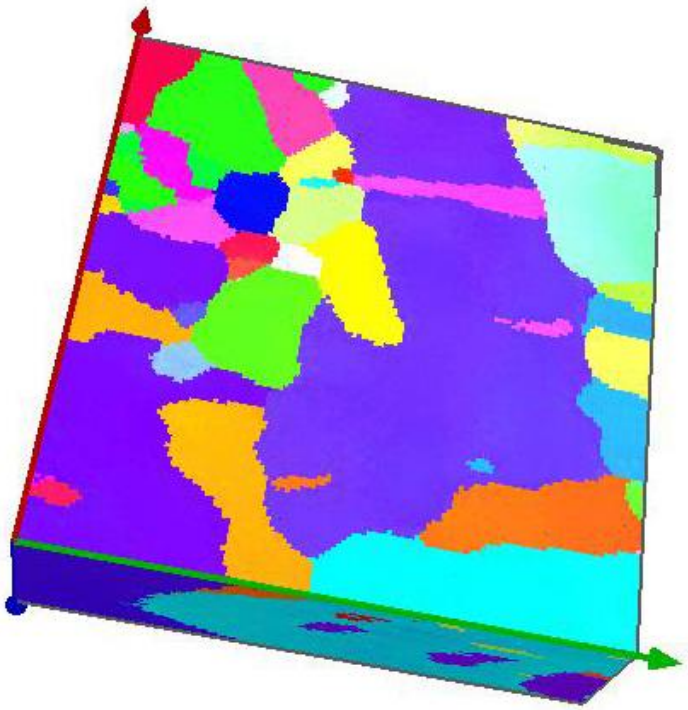

Fig. 4 3D EBSD reconstruction of an RT annealed microstructure

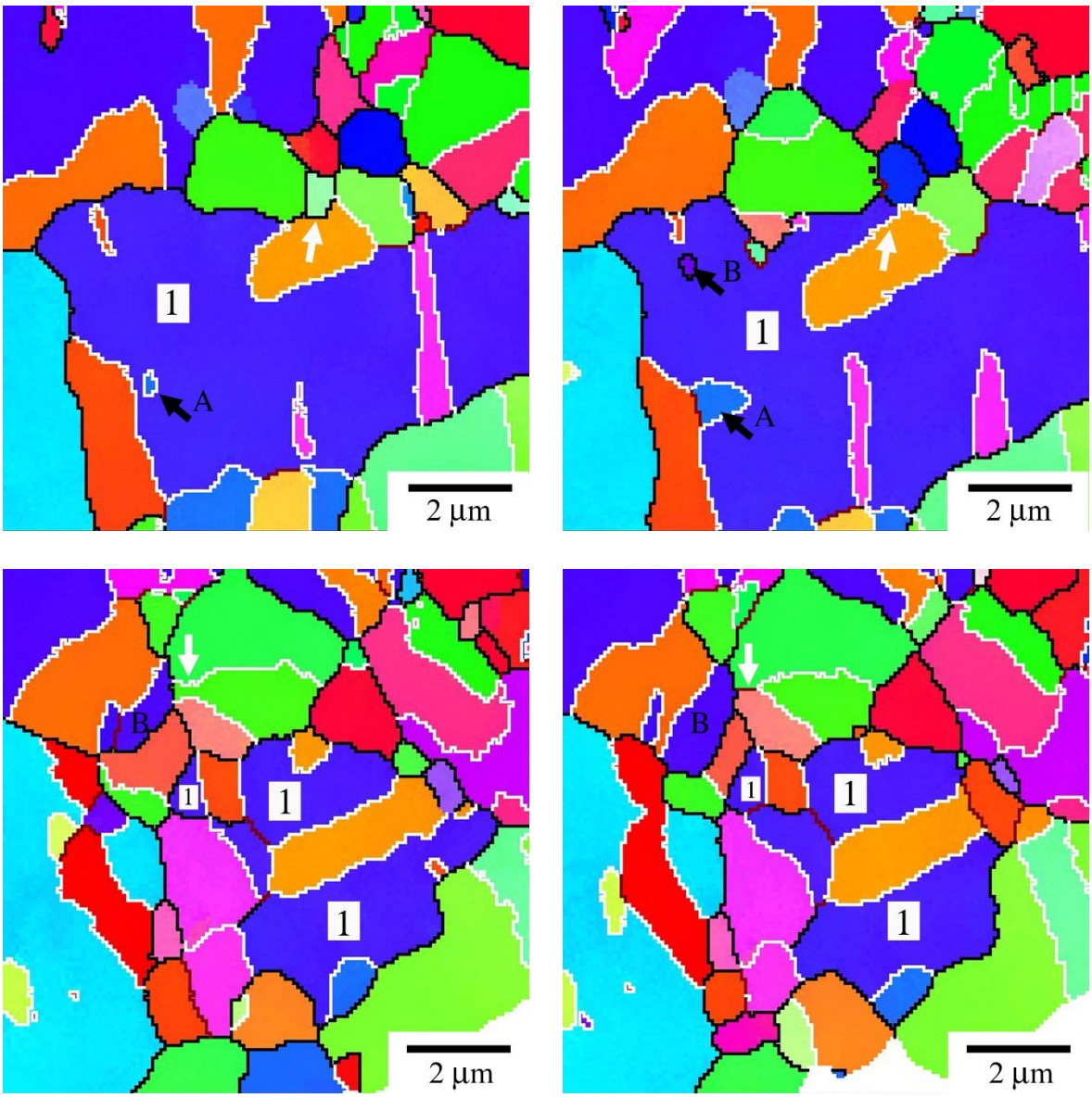

Fig. 5 Selected 2D slices from a 3D EBSD map (Fig. 4). Coloured boundaries indicate special boundaries (Σ3 white, Σ9 brown), black boundaries indicate random boundaries.

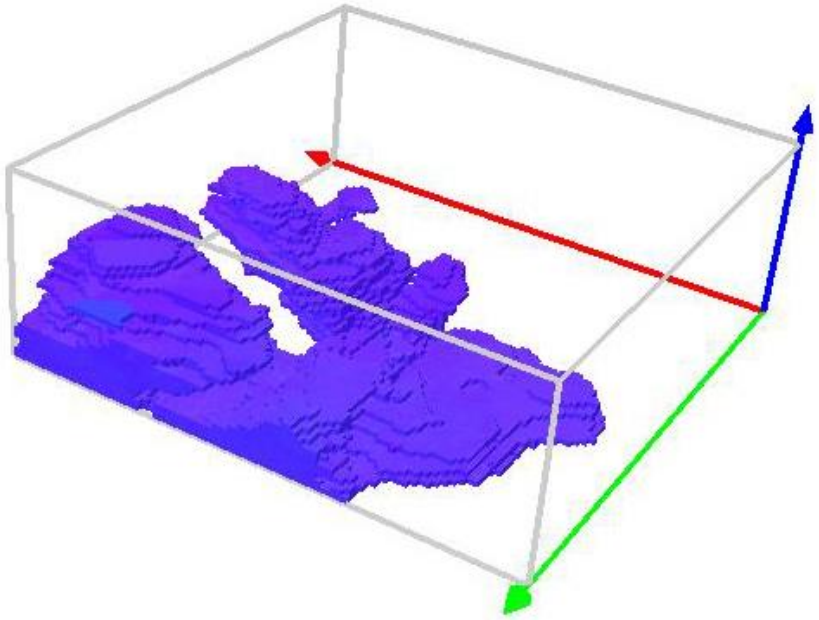

Fig. 6 Grain 1 from the 3D EBSD map reconstructed from 2D slices

Fig. 7 3D microstructure of pure Cu after HPT and long-term annealing (grains coloured at random).

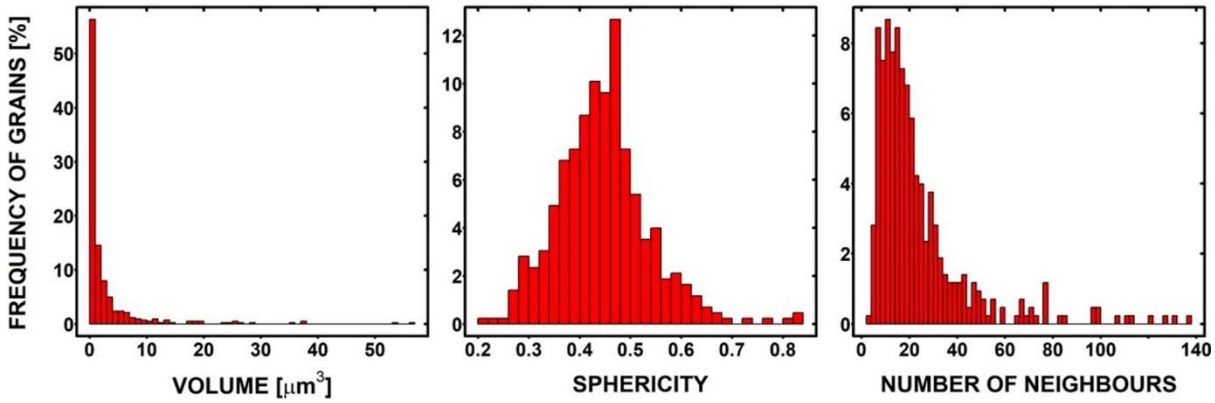

Fig. 8 Histograms of 3D grain characteristics of the sample shown in Fig. 7: volume [μm^3], sphericity, number of neighbours.

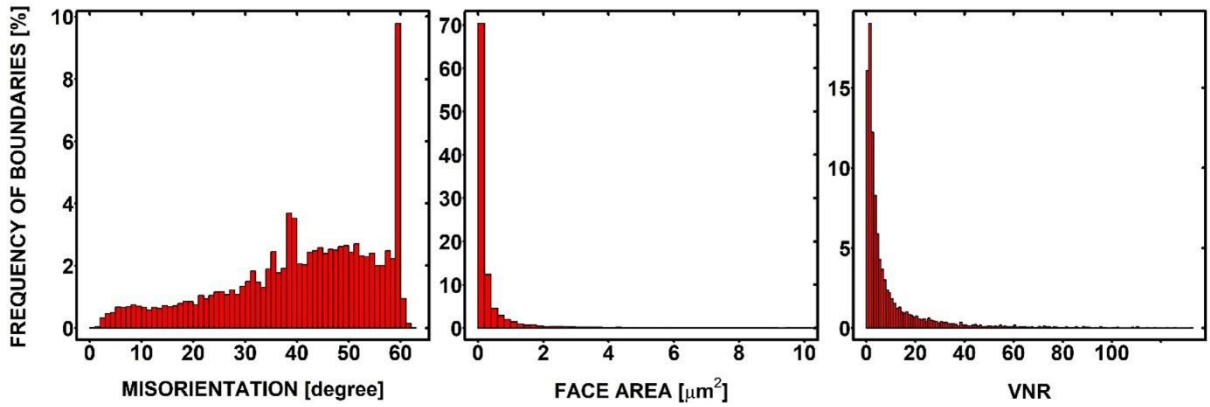

a)

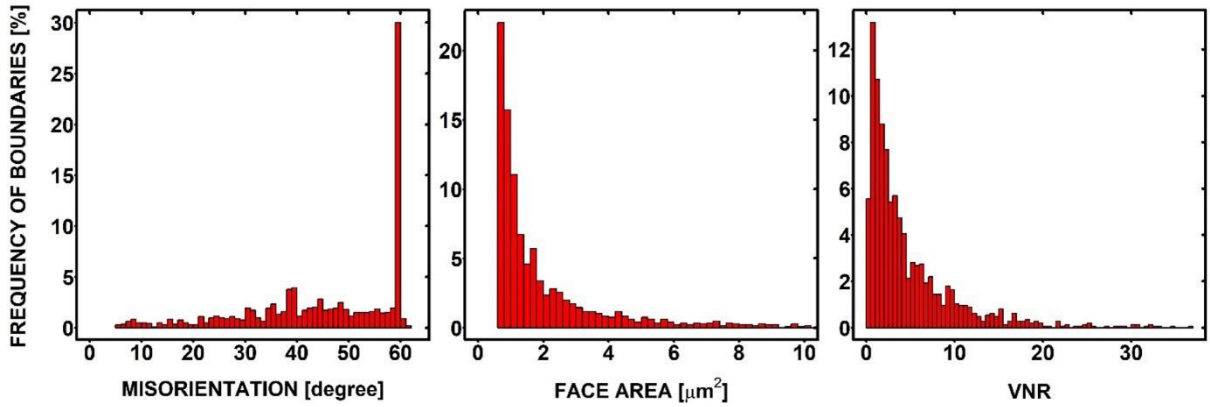

b)

Fig. 9 Histograms of 3D characteristics of grain boundaries (faces) of the sample shown in Fig. 7: misorientation [degrees], surface area [μm^2], VNR defined in (2). The histograms are computed a) from all 11513 faces, and b) from the 1458 faces with the biggest surface areas. The largest surface is 67.83 μm^2, but only 40 faces have surface area larger than 10 μm^2. Therefore histograms of face area do not display 0.35 % of faces in the case a) and 2.74 % of faces in the case b).

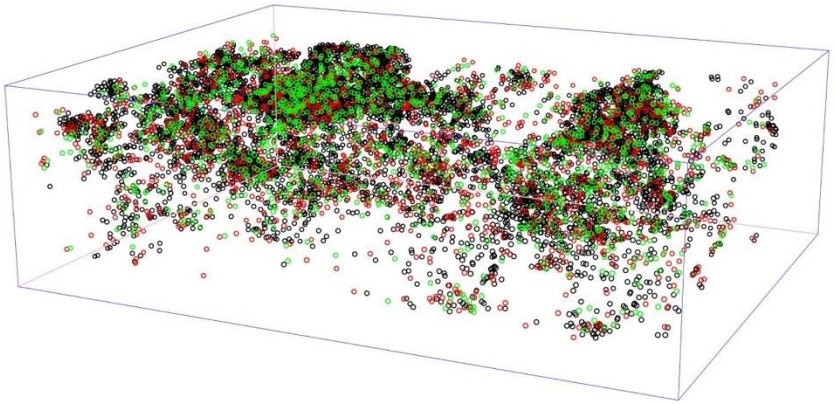

Fig. 10 3D plots of the point patterns (I) – red, (II) – green and (III)-black, corresponding to the locations of grain faces.

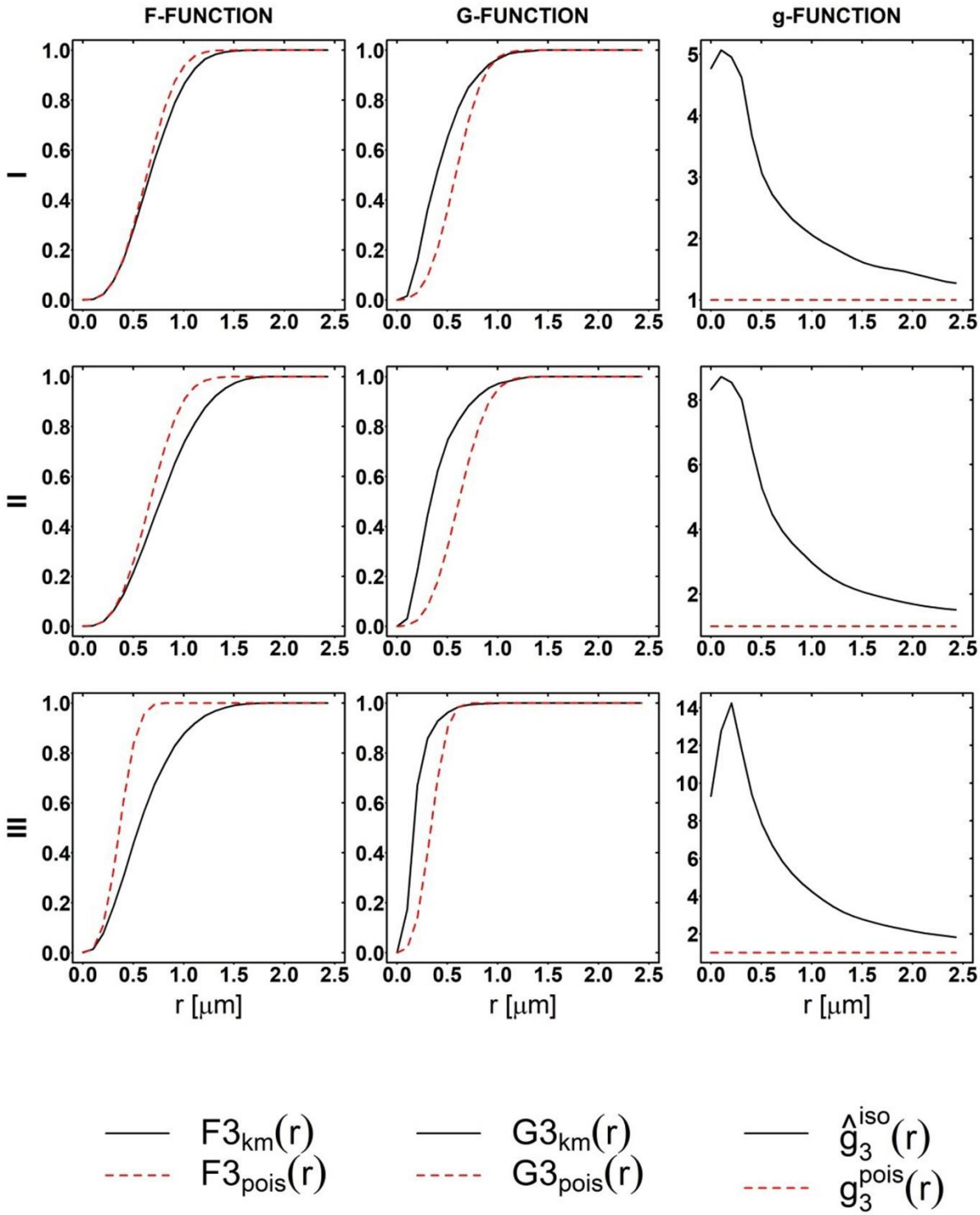
F-FUNCTION
G-FUNCTION
g-FUNCTION
I
II
III
r [μm]
r [μm]
r [μm]
F3km(r)
F3pois(r)
G3km(r)
G3pois(r)
ĝ3iso(r)
g3pois(r)

Fig. 11 Spatial distribution of grain boundaries: F-function, G-function and g-function of the point patterns (I), (II), and (III) (estimated with correction of edge effects, solid lines) and of the completely random model (dashed lines).

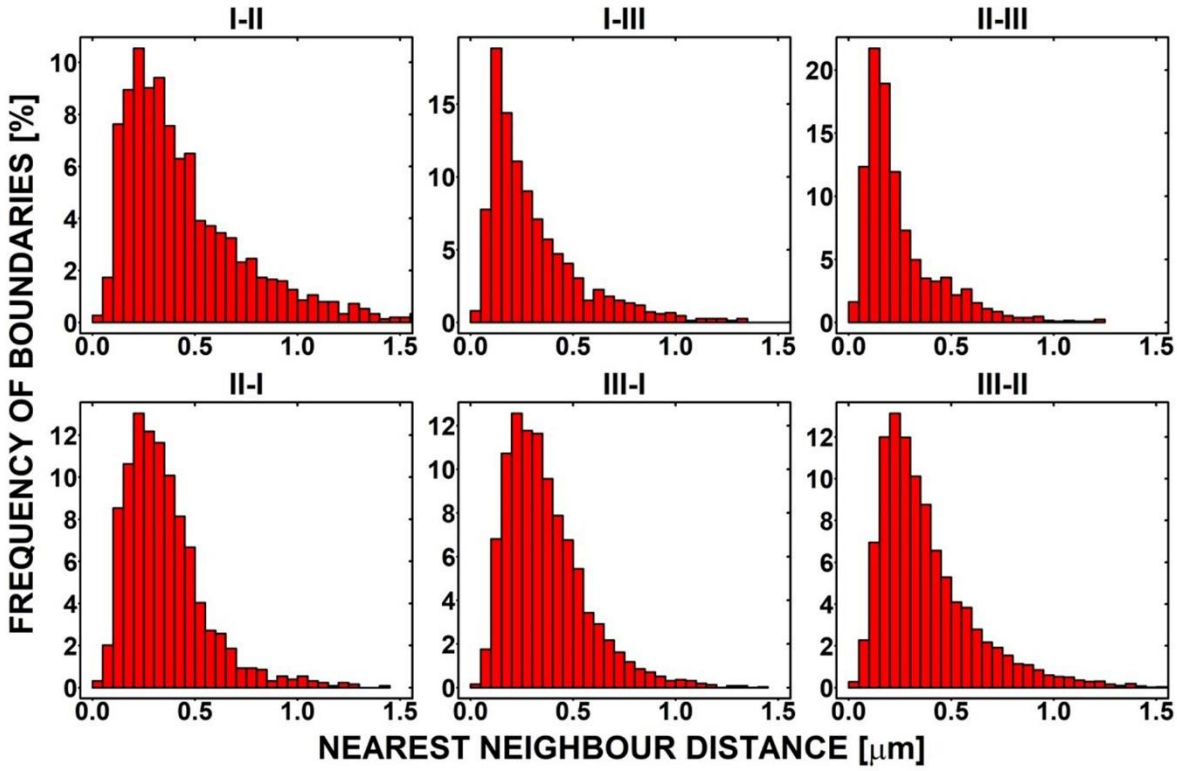

Fig. 12 Histograms of cross-nearest-neighbour distances, for pairs of points from (I), (II), and (III). The heavier tail in histogram I-II in comparison to histogram II-I indicates that pattern (II) is slightly more clustered than (I). Note that the histograms regarding pattern (III) are influenced by a larger difference between the number of points of the respective pairs of point patterns.

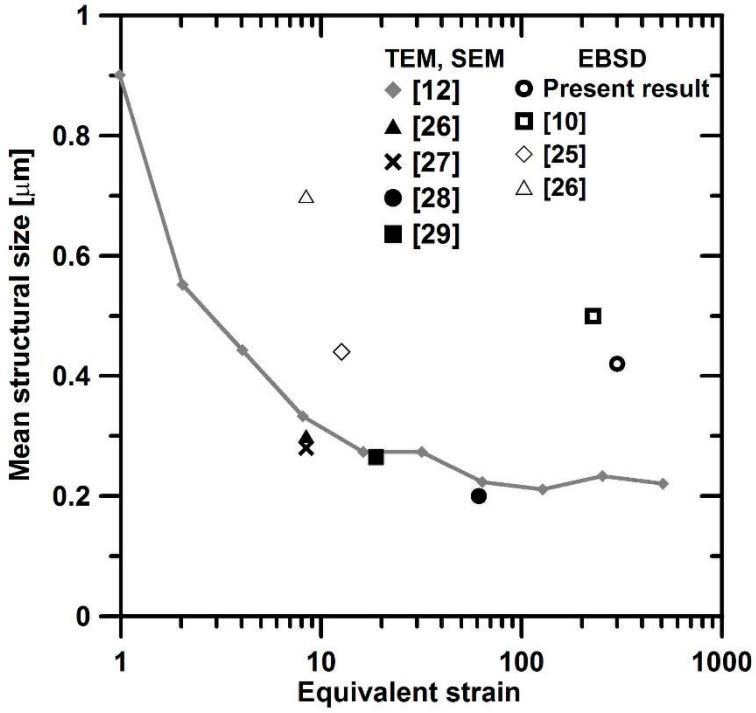

Fig. 13 Comparison of mean grain size measured in the present work with results published in previous works

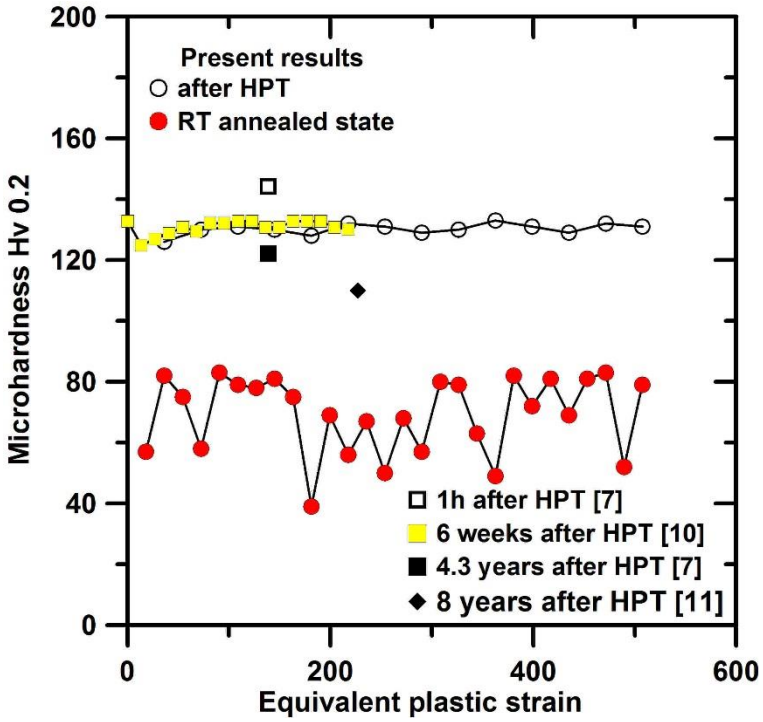

Fig. 14 Comparison of microhardness measured in the present work with results published in previous works